Biophysical Journal Volume 98 June 2010 2933–2942

Crystal Structure and Trimer-Monomer Transition of N-Terminal Domain of EhCaBP1 from *Entamoeba histolytica*

Shivesh Kumar,[†] Ejaz Ahmad,[‡] M. Shahid Mansuri,[†] Sanjeev Kumar,[†§] Ruchi Jain,[†] Rizwan Hasan Khan,[‡] and S. Gourinath[†*]

[†]School of Life Sciences, Jawaharlal Nehru University, New Delhi, India; [‡]Interdisciplinary Biotechnology Unit, Aligarh Muslim University, Aligarh, India; and [§]Department of Biochemistry, Jamia Hamdard, Hamdard Nagar, New Delhi, India

ABSTRACT EhCaBP1 is a well-characterized calcium binding protein from *Entamoeba histolytica* with four canonical EF-hand motifs. The crystal structure of EhCaBP1 reveals the trimeric organization of N-terminal domain. The solution structure obtained at pH 6.0 indicated its monomeric nature, similar to that of calmodulin. Recent domain-wise studies showed clearly that the N-terminal domain of EhCaBP1 is capable of performing most of the functions of the full-length protein. Additionally, the mode of target binding in the trimer is similar to that found in calmodulin. To study the dynamic nature of this protein and further validate the trimerization of N-terminal domain at physiological conditions, the crystal structure of N-terminal domain was determined at 2.5 Å resolution. The final structure consists of EF-1 and EF-2 motifs separated by a long straight helix as seen in the full-length protein. The spectroscopic and stability studies, like far and near-ultraviolet circular dichroism spectra, intrinsic and extrinsic fluorescence spectra, acrylamide quenching, thermal denaturation, and dynamic light scattering, provided clear evidence for a conversion from trimeric state to monomeric state. As the pH was lowered from the physiological pH, a dynamic trimer-monomer transition was observed. The trimeric state and monomeric state observed in spectroscopic studies may represent the x-ray and NMR structures of the EhCaBP1. At pH 6.0, the endogenous kinase activation function was almost lost, indicating that the monomeric state of the protein, where EF-hand motifs are far apart, is not a functional state.

INTRODUCTION

Entamoeba histolytica is a widely distributed parasitic protozoa and the major cause of morbidity and mortality in developing countries (1–3). The genome of *E. histolytica* contains numerous calcium binding proteins (4,5). The calcium binding protein-1 from *E. histolytica* (EhCaBP1), is an essential effector for cytoskeletal organization and is vital for survival of the organism (6). EhCaBP1 contains four EF-hand motifs, each of which binds to one calcium ion. The crystal structure of EhCaBP1 was published from our laboratory at 2.4 Å resolution, where only the N-terminal half of the molecule was traced (7). The solution structure reported at a low pH (pH 6.0) indicated its monomeric nature and structural similarity with calmodulin (CaM) (8,9). Unlike CaM, the crystal structure of EhCaBP1 showed that the EF1 and EF2 are far apart and connected by a long straight helix (7). The crystal structure displayed the domain-swapped trimeric arrangement of EF-hand motifs of the N-terminal domain; the assembled-domain in the trimer is similar to the N-terminal domain of CaM (7).

Recent studies on the independent domains of EhCaBP1 have shown that the N-terminal domain can carry out most of the functions of full-length protein (10). The N-terminal domain activates the endogenous kinase more efficiently than the full-length protein (10,11). Fluorescence microscopic study indicated the maximum colocalization of Nt-EhCaBP1 with F-actin at the phagocytic cup (10), and less with the full-length molecule in the cytoplasm (6). The C-terminal domain of EhCaBP1 shows reduced kinase activity of ~50–60% of the full-length protein and is localized in the cytoplasm with no specific relation with F-actin or phagocytic cup (10). The crystal structure of EhCaBP1-Phe complex shows that the phenylalanine is bound at the assembled-domain interface, revealing its target binding mode (10). These studies show clearly that the N-terminal domain carries out most of the functions in comparison to the full-length EhCaBP1. Despite its low sequence identity, the NMR structure of EhCaBP1 more closely resembles that of CaM (8). To further validate the trimerization of the N-terminal domain at a physiological condition, monomeric state at lower pH, and also to study the dynamic behavior of this molecule, the N-terminal domain of EhCaBP1 (Nt-EhCaBP1) was overexpressed, purified, crystallized, and the three-dimensional structure was determined. We believe the studies reported here provide evidence for the dynamic nature of Nt-EhCaBP1, depending on the pH of the environment. The far and near-ultraviolet (UV) circular dichroism (CD) spectroscopy, intrinsic tyrosine fluorescence, acrylamide quenching of tyrosine fluorescence, and ANS binding studies confirm the transition of trimer to monomer from pH 7.4 to pH 6.0. The physiological condition is more favorable for its trimeric organization, whereas the low pH leads to the dissociation of trimer to its monomeric units. Due to its inability to activate endogenous kinase at pH 6.0, the monomeric state is not the active conformation of this protein.

Submitted December 4, 2009, and accepted for publication March 22, 2010.

*Correspondence: sgourinath@mail.jnu.ac.in

Editor: Kathleen B. Hall.

0006-3495/10/06/2933/10 $2.00

doi: 10.1016/j.bpj.2010.03.048

MATERIAL AND METHODS

Buffers and solutions

Throughout the spectroscopic experiments, only two solution conditions were used: solution I (similar to physiological condition): 20 mM Tris-HCl pH 7.4, 1 mM $CaCl_2$, 150 mM NaCl; and solution II (similar to NMR experimental condition): 20 mM Bis-Tris-HCl pH 6.0, 1 mM of $CaCl_2$. All solutions were prepared in MilliQ water and filtered through a 0.2-μm Millipore syringe filter. pH measurements were carried out using EUTECH instruments-pH 510.

Overexpression and purification of N-terminal domain of EhCaBP1

The clone of N-terminal domain in pET3c expression vector was the gift of Prof. Alok Bhattacharya (School of Life Sciences, Jawaharlal Nehru University, New Delhi). The N-terminal domain consisted of the first 66 amino acids of the full length protein, which is 134 amino acids in length. The N-terminal domain of EhCaBP1 was expressed and purified in a manner similar to that of full-length protein (12), with minor changes. The DEAE-Sepharose column was washed with 10 bed-volumes of 50 mM of Tris-Cl (pH 7.5), 2 mM EGTA (pH 7.5) and 10 bed-volumes of 50 mM of Tris-Cl (pH 7.5), 2 mM EGTA (pH 7.5) and 20 mM of NaCl. The protein was eluted in 1-mL fractions with 50 mM Tris-Cl (pH 7.5), 3 mM $CaCl_2$, and the absorbance at 280 nm was monitored. Centricon tubes from Millipore (3 kDa cut-off size) were used to concentrate the protein; the final concentration of the protein was measured using Bradford assay (13).

Mass spectroscopy of N-terminal domain of EhCaBP1

Mass spectroscopy was done using an in-house Bruker Daltonics flex Analysis instrument of type autoflex TOF-TOF. The purified protein solution was mixed (1:1) with matrix (sinapinic acid in acetonitrile containing 0.1% TFA) on a target plate and left to dry before analysis by MALDI-MS. The mass scale of the instrument was externally calibrated using calibration mixture (bradykinin, angiotensin I, angiotensin II, substance P, bombesin, renin substance, ACTH clip, and somatostatin).

Crystallization of Nt-EhCaBP1

The purified N-terminal protein was concentrated to 15 mg/mL in 50 mM Tris buffer (pH 7.5) containing 3 mM $CaCl_2$ and 20 mM of NaCl for crystallization trials. Initial crystallization screenings were carried out at both 16°C and 4°C using hanging-drop method with equal ratios (3 μL) of protein and precipitant solution. Nt-EhCaBP1 crystals appeared within 2–3 days in 18% PEG 500 MME, 100 mM acetate buffer pH 3.6–3.8 with small and round-shaped morphology (Fig. S2 *A* in the Supporting Material), whereas the crystals that appeared in 15–18% PEG 400, 5 mM $CaCl_2$, 10% Isopropanol, 50 mM NaCl and 100 mM acetate buffer pH 3.6–4.2 were thin needles (Fig. S2 *B*). The rod shaped diffractable quality crystals ($150 \times 150 \times 100$ μm^3) appeared at 16°C in approximately 7–10 days on addition of 100 mM of KCl solution and a mixture of 1 mM each of glycine, proline, glucose, and sucrose as an additive to the PEG 400 crystallization condition (Fig. S2 *C*).

Data collection, processing, and structure determination

The x-ray diffraction experiments were carried out at 100 K with N-terminal crystals mounted on cryo-loops in mother liquor and were flash-frozen in liquid nitrogen. These crystals diffracted to 2.5 Å with an in-house rotating anode generator (MICROSTAR, Bruker AXS). The data set was indexed, processed, and scaled with an Automar program (Marresearch, Norderstedt, Germany) (Table 1).

The structure was solved by molecular replacement with Phaser program (14) using the native structure of EhCaBP1 (2NXQ) as the search model. In the native structure only N-terminal domain (2–67 amino acids) was traced and whole C-terminal domain (68–134) was missing. The structure was refined to 2.5 Å resolution by iterative model building using COOT graphics package (15) combined with conjugate-gradient minimization with bulk solvent correction in CNS (16) and PHENIX (17) (Table 1).

CD measurements

The isothermal studies and thermal denaturations of Nt-EhCaBP1 by CD measurements were carried out with Chirascan, a polarimeter of Applied-Photophysics equipped with a QUANTUM N.O.R.T.H.W.E.S.T.-TC125, a Peltier-type temperature controller. The instrument was calibrated with d-10-camphorsulfonic acid (18). All the isothermal CD measurements were made at 25°C. Spectra were collected with 20 nm/min scan speed, 0.1 nm data pitch, and a response time of 2 s. Each spectrum was the average of 10 scans. The Far-UV CD spectra (200–250 nm) were taken at protein concentrations of 27 μM in a cell of 0.1 cm path length; for near-UV CD spectra (250–300 nm), 145 μM protein and 1 cm path length cell were taken. The results were expressed as MRE (mean residue ellipticity) in deg $\times$ $cm^2 \times dmol^{-1}$, which is given by:

$$\mathrm{MRE} = \theta_{obs}(\mathrm{mdeg})/10 \times n \times C\mathrm{p} \times l, \qquad (1)$$

where θ_{obs} is the observed ellipticity in degrees, Cp is the molar fraction, and l is the length of the light path in centimeters. All spectra were smoothed by the Savitzky-Golay method with 25 convolution width.

The thermal denaturations were studied in the range of 293–363 K with 1 K increment and 1 K $\times$ min^{-1} temperature slope probed by far-UV CD at 222 nm and near-UV CD at 280 nm. The curves were normalized, assuming a linear temperature dependence of the base lines of native and denatured states.

Steady-state fluorescence measurements

Intrinsic and extrinsic fluorescence studies were carried out on a Cary Eclipse fluorescence spectrophotometer equipped with a constant temperature holder at 25°C with a 1 cm path-length cell. The excitation and emission slits were both set at 5 nm. The concentration of protein was maintained at 3.5 μM. Intrinsic fluorescence was measured by exciting tyrosine at 275 nm, and emission spectra were recorded in the range of 300–400 nm in both solution conditions. For extrinsic fluorescence, 1-anilino-8-naphthalene sulfonate (ANS) was probed. The concentration of ANS stock solution was determined using a molar absorption coefficient (ε) of 5000 $M^{-1} \times cm^{-1}$ at 350 nm. In the ANS binding experiments, the excitation was set at 380 nm, and the emission spectra were taken in the range of 400–600 nm.

For all spectra, the smoothing parameters, namely function type, smoothing order, number of points, and number of times, were Savitzky-Golay, 4, 20, and 1, respectively.

Acrylamide quenching experiments

Aliquots of 1 M acrylamide stock solution were added to the Nt-EhCaBP1 solution (3.5 μM) to achieve the desired range of quencher concentrations (0.01–0.1M). Excitation was set at 275 nm and the emission spectrum was recorded in the range of 300–400 nm. The decrease in fluorescence intensity at the corresponding wavelength (λ em =305 nm) was analyzed according to the Stern-Volmer equation:

$$F_0/F = 1 + K_{sv}[Q], \qquad (2)$$

where F_0 and F are the fluorescence intensities at an appropriate wavelength in the absence and presence of quencher Q and K_{sv} is the Stern-Volmer

TABLE 1 Crystallographic data-statistics of Nt-EhCaBP1

Data set	Nt-EhCaBP1
Crystallographic data	
X-ray source	Microstar
Wavelength	1.5418
Space group	P3
Unit cell parameters (Å)	
a	89.583
b	89.583
c	35.049
Resolution range(Å)	22.0–2.5
R_{sym} (%)	4.06 (26.1)
Completeness	99.0 (99.5)
Observations (*N*)	39,681
Unique observations (*N*)	10,746
Redundancy	3.7
Average I/s(I)	10.5 (1.5)
Crystal mosaicity (°)	0.4
Refinement	
Resolution	22.0–2.5
R-factor (%)	23.1
Free R-factor (%)	28.7
Mean B-factor(Å^2)	52.1
Atoms (*N*)	
Protein	2011
Ca	8
Water	64
RMS deviations	
Bonds (Å)	0.010
Bond angles (°)	1.12
Dihedral angles (°)	19.3
Cross validated error (Luzzati plot, Å)	0.35
Cruickshanks DPI for coordinate error	0.316

DPI, diffraction component precision index; RMS, root mean-square. Values in parentheses are for the last resolution shell. Free R-factor was calculated with a subset of 9.5% randomly selected reflections.

collisional quenching constant. As there are two tyrosine residues in this protein, they may be differentially exposed to the quencher; hence, a modified Stern-Volmer equation was applied:

$$F_0/F_0 - F = 1/(K_{sv}[Q]fa) + 1/fa, \quad (3)$$

where *f*a is the fraction of tyrosine residues accessible to the quencher (19).

Dynamic light scattering measurements

Dynamic light scattering (DLS) measurements were carried out at 830 nm using DynaPro-TC-04 dynamic light scattering equipment (Protein Solutions, Wyatt Technology, Santa Barbara, CA) equipped with a temperature-controlled microsampler. The protein concentration was 5 mg/mL in two different solution conditions. The protein samples were spun at 10,000 rpm for 10 min and were filtered through 0.02 μm Whatman syringe filter directly into a 12-μL quartz cuvette. For each experiment, 20 measurements were taken. Mean hydrodynamic radius (R_H), standard deviation, polydispersity, and percent of peak area were analyzed using Dynamics 6.10 software using the optimized resolution. (R_H) was calculated from translation diffusion coefficient by Stokes-Einstein relationship.

In vitro kinase assay

Total *Entamoeba* cell extract was prepared and the activity of EhCaBP1-dependent kinases was estimated as described previously (20). Two moles of either full-length EhCaBP1 or NtEhCaBP1 was added at different pH conditions. The gels were dried and exposed to an imaging plate and the intensity of the band was measured with densitometry.

RESULTS AND DISCUSSION

Overall structure of N-terminal domain of EhCaBP1

The Nt-EhCaBP1 was purified and crystallized as mentioned in Material and Methods. The crystallization condition is completely different from that of the full-length protein. The full-length EhCaBP1 crystals were only obtained when 2-methyl-2,4-pentandiol was used as a precipitant and belonged to $P6_3$ space group (7). The hexagonal crystals of Nt-EhCaBP1 were obtained in PEG 400 (Fig. S2). Nt-EhCaBP1 crystals were confirmed by washing the crystals with mother liquor and by molecular weight determination on SDS-PAGE and MALDI mass spectrometry (Fig. S1). The data were collected using an in-house x-ray source. The crystals belonged to P3 space group, with four molecules in the asymmetric unit. The structure was solved by molecular replacement with a Phaser program (13), using the native structure of EhCaBP1 (2NXQ) as the search model. The final model refined well with good electron density and crystallographic R-factor, and R-free values fell within the range of average values for structures refined at this given resolution (21). A summary of the data collection statistics is given in Table 1. Two EF-hand motifs were separated by a long helix, similar to that traced from the full-length protein with one calcium-ion bound at each EF-hand motifs (Fig. 1 *A*). The coordination geometry of both the calcium-binding loops is shown in Fig. 1, *B* and *C*. The calcium ion coordinates with seven of its ligands, including one water molecule, in a pentagonal bipyramidal fashion.

Symmetry-related trimeric structure of N-terminal domain

The extended conformation of N-terminal domain formed a domain-swapped trimer, where three symmetry-related molecules interacted in a head-to-tail manner similar to that reported for a full-length protein structure, revealing trimerization of N-terminal domain (7). EF-hand 1 of one molecule interacted with EF-hand 2 of the symmetry-related molecule to form a trimer (Fig. 1 *D*). The assembled-domains of this trimeric organization were structurally similar to N-terminal domain of CaM and N-terminal domain of NMR structure of EhCaBP1 (Fig. 1 *E*).

CD measurements

The protein secondary structure changes were estimated by observing far-UV CD spectra. Two deep minima near 208 nm and 222 nm are characteristic of α-helical structure

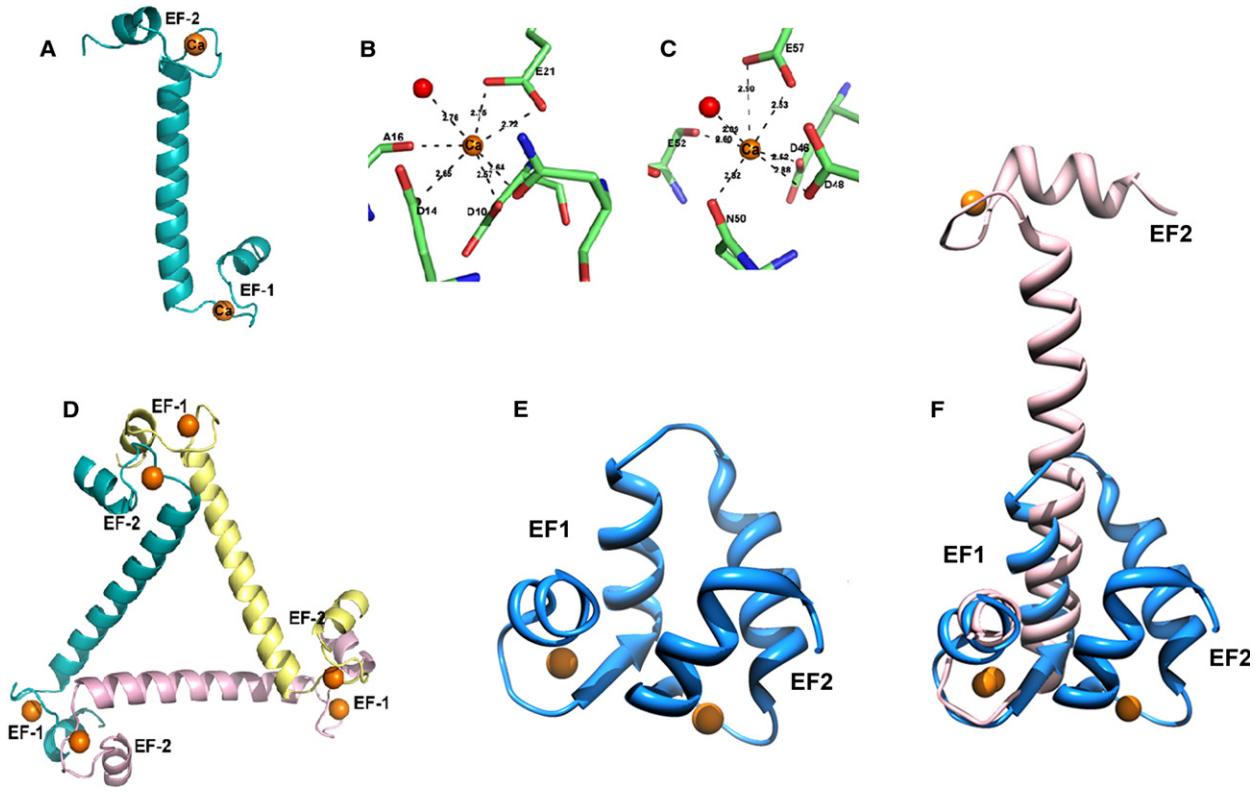

FIGURE 1 (*A*) Crystal structure of N-terminal domain shows the extended conformation, where EF-hand 1 and EF-hand 2 motifs are far apart and each motif binds one calcium ion (*orange sphere*). The linker region between the two motifs forms a long straight helix. (*B*) Ca^{2+}-coordination in calcium-binding loop 1. (*C*) Ca^{2+}-coordination in calcium-binding loop 2. The coordination distances are shown in Å. Calcium and water molecules are shown as orange and red spheres, respectively. (*D*) Three symmetry-related molecules interact with each other and results in trimeric organization. Three N-terminal molecules are shown in three different colors with the bound calcium ions as orange spheres. The EF-hand1 of one molecule interacts with EF-hand 2 of the neighboring molecule to form the domain. (*E*) N-terminal domain from the NMR structure of EhCaBP1 (1JFK), where EF-hand 1 and EF-hand 2 motifs interact with each other within the same chain and forms a domain. (*F*) Crystal structure (*pink*) and NMR structure (*blue*) of NtEhCaBP1 were superposed on each other. The EF1 motif superimposed well and the orientation of EF2 completely different in crystal structure compared to NMR structure, due to the differences in the structure of linker region. The graphics were generated by PyMOL (30).

in aqueous solution due to π-π* & n-π* transitions, respectively. From Fig. 2 *A*, significant, defined α-helical structures were detected for Nt-EhCBP1 in both solutions with different intensities. As the pH decreased, a notable rearrangement of spectrum occurred with lowering in major minima as well as slight changes in the shape of spectra. A lowering in negative value of ellipticity at 208 nm and 222 nm indicated a sign of α-helical reduction due to intramolecular H-bonding rearrangement. This pH-induced alteration of secondary structure was quantified by K2D online software, an algorithm-based neural network software (22,23). On lowering the pH from 7.4 to 6.0, the α-helical content dropped by 17% and the β-sheet (7%) and random coil (11%) increased. Spectra scanned in different solution conditions of different pH ranging from 7.4 to 6.0 (data not shown). A single isodichroic point was obtained near 203 nm, indicating a two-state transition between oligomeric to monomeric states with altered secondary structures, although the shapes of all spectra were very similar, with varying minima at 208 nm and 222 nm.

The protein Nt-EhCaBP1 consists of five phenylalanine and two tyrosine residues, but no tryptophan or cysteine residues. Hence, the peaks and shoulders in the near-UV CD spectrum correspond to only phenylalanine and tyrosine residues in different microenvironments. Phe^{6} and Phe^{58}, at the interface of the trimer, were significantly affected in the structural transition from trimeric to monomeric form (Fig. 1 and Fig. 4). The fine peaks at 259.8 nm and 263 nm were caused by Phe residues. In solutions I and II, the peaks at ~260 suggest that Phe^{6} of EF-1 and Phe^{58} of EF-2 were in different environments in these conditions. The peak at 263 nm may have been caused by Phe residues of the same domain, as they were almost unaffected, even on lowering of the pH. In Fig. 2 *B*, the near-UV CD spectrum also had an abrupt loss of sharp features at lower pH, indicating the loss of specific tertiary structures in condition II as compared to condition I. Tyr^{19} present at the interface of the trimer may be extremely sensitive to different pH conditions (Fig. 2 *B*). This may also explain the differences in the near-UV CD spectra.

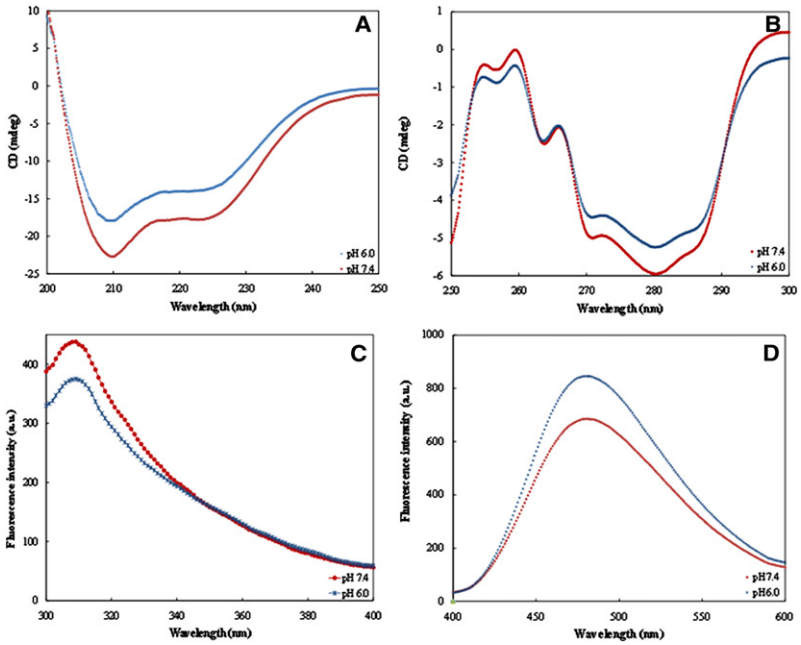

FIGURE 2 (*A*) Far-UV CD spectra. (*B*) Near-UV CD spectra. (*C*) Tyrosine fluorescence spectra. (*D*) ANS fluorescence spectra of Nt-*Eh*CBP1 in solution I (•) and solution II (*). Details are given in Material and Methods.

Steady-state fluorescence measurements

In intrinsic fluorescence of proteins, the degree of tyrosine exposure to solvent can be determined by the λ_{max} and fluorescence intensity as the loosely packed or denatured state of proteins show less fluorescence intensity along with red shifted spectra. This means that tyrosine fluorescence maxima are dependent on the hydrophobicity of the surrounding environment. Fig. 2 *C* shows the emission spectrum of Nt-EhCBP1 at different solution conditions. The maximum emission at physiological pH (solution I) was at 307 nm with fluorescence intensity of 427 ± 6 (a.u.), indicating the burial of tyrosine residues. On decreasing pH (solution II), there occurred a red shift in λ_{max}, which was clear evidence of variability in the immediate hydrophobic microenvironment of tyrosine and the conformational states of respective protein owing to structural changes. Here, on lowering the pH, the red shift in λ_{max} and decreased intensity (363 ± 7 a.u.) indicate a comparatively higher hydrophilic environment that may have occurred due to structural changes and partial exposure of Tyr to the solvent.

8-Anilino-1-naphthalenesulfonic acid (ANS) is an extrinsic fluorescent probe that binds to the hydrophobic sites of proteins (23). This property is frequently used as a probe to study the protein's conformational changes and measure its hydrophobic surfaces accessibility (24). Binding of ANS to the hydrophobic regions of protein increases fluorescence intensity and creates a significant blue shift of fluorescence maximum, which has been used widely to detect nonnative, intermediate conformations of different proteins. Comparative emission fluorescence spectra of Nt-EhCaBP1 in different solution conditions are shown in Fig. 2 *D*. As seen in the figure, ANS fluorescence was lower in solution I however, with a decrease in pH (solution II), ANS intensity increased, along with a momentous blue shift in fluorescence maximum (Table 2). The blue-shifted fluorescence indicates the availability of hydrophobic patches at lower pH due to the disorganization of secondary, tertiary, and quaternary

TABLE 2 Spectroscopic biophysical properties of monomer and trimer of Nt-EhCaBP1

Variables	Trimer	Monomer
Solution condition	I: pH 7.4 (+)1 mM $CaCl_2$ (+)150 mM NaCl	II: H 6.0 (+)1 mM $CaCl_2$ (−)150 mM NaCl
Far-UV CD		
$MRE_{222\ nm}$	−20,128 ± 110	−15,854 ± 90
Secondary structures (%)		
α-helix	78 ± 4	61 ± 2
β-sheet	1 ± 0.4	07 ± 0.9
Random coil	21 ± 1	32 ± 2
Near-UV CD		
$MRE_{280\ nm}$	−71 ± 3	62 ± 2
Tyrosine fluorescence		
$F.I._{305nm}$	427 ± 6 (a.u.)	363 ± 7 (a.u.)
λ_{max}	308 nm	309 nm
ANS binding		
$F.I._{480nm}$	685 ± 12 (a.u.)	846 ± 8 (a.u.)
λ_{max}	483 nm	479 nm
Acrylamide quenching		
K_{sv}	13.3 ± 0.4 M^{-1}	15.4 ± 0.6 M^{-1}
fa	1.01 ± 0.1	1.9 ± 0.3
Dynamic light scattering		
R_H	3.0 ± 0.4 nm	1.1 ± 0.1 nm
%Pd	4.3 ± 2.2	8.6 ± 3.1

CD, circular dichroism; *fa*, fraction accessibility; F.I., fluorescence intensity; K_{sv}, Stern-Volmer constant; MRE, mean residual ellipticity in deg × cm^2 × $dmol^{-1}$; Pd, polydispersity; R_H, hydrodynamic radii; UV, ultraviolet.

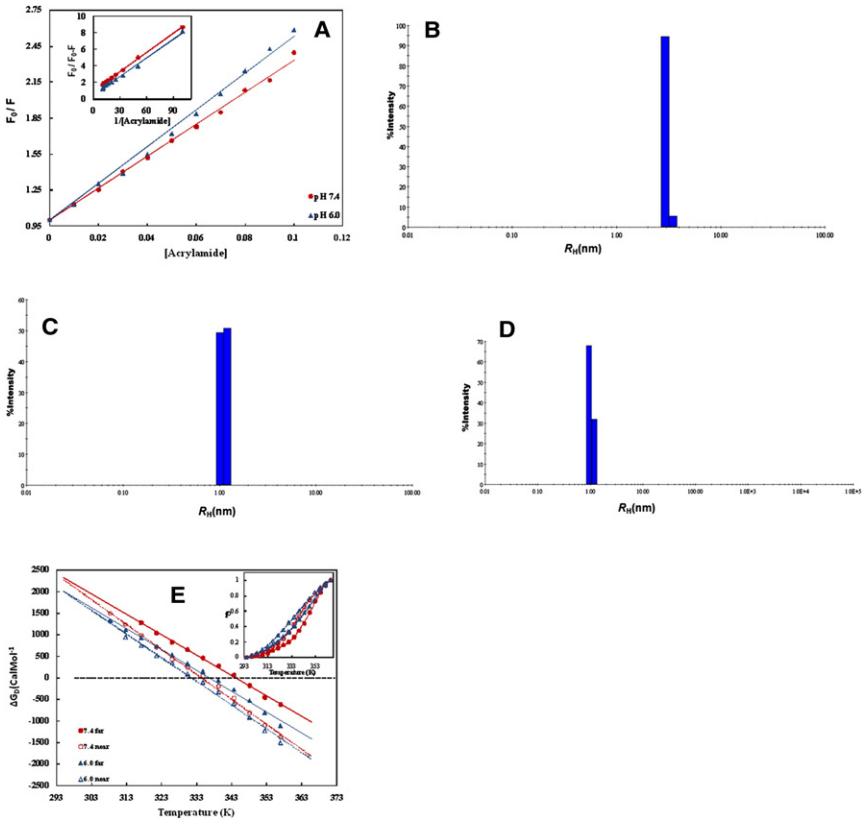

FIGURE 3 (*A*) Stern-Volmer and modified Stern-Volmer (*inset*) plot for acrylamide quenching of Nt-EhCBP1 in solution I (●) and solution II (▲). (*B*) R_H determination by DLS in solution I; (*C*) in solution II; and (*D*) in solution I with 20% ethanol. (*E*) Plot of ΔG_D versus temperature for thermal denaturation of Nt-EhCBP1 in solution I (●) and solution II (▲) by far-UV CD (*solid*) and near-UV CD (*open*). (*Inset*) f_D is plotted against temperature. For more detail, see Material and Methods.

structures of protein; suggesting that ANS must be binding to those regions. At physiological condition, the protein hydrophobic patches were less exposed; when pH was reduced, the hydrophobic residues were relatively more exposed to solvent, suggesting that Nt-EhCaBP1 is in different structural state in two different conditions. At pH 7.5, the protein is to some extent in a packed state; at pH 6.0, it is in a loosely folded conformation with exposed hydrophobic regions.

Acrylamide quenching

The fluorescence properties of tyrosine residues can be used to obtain topological information about proteins. Fluorescence quenching of the tyrosine residues by neutral quencher (acrylamide) provides information about the solvent accessibility of these residues in proteins and the polarity of their microenvironment. Fig. 3 *A* depicts the Stern-Volmer plot and modified Stern-Volmer plot (inset) for acrylamide quenching studies carried out in solutions I and II. The values of the Stern-Volmer constant (K_{sv}) and fractional accessibility of tyrosine residues to quencher (*f*a) were calculated from the plot (Table 2). K_{sv} for Nt-EhCaBP1 in solution condition I (K_{sv} =13.3 ± 0.4 M^{-1}) was lower than that of solution condition II (K_{sv} =15.4 ± 0.6 M^{-1}) and was accompanied by an increase of *f*a from 1.01 (solution I) to 1.88 (solution II). These results indicated that tyrosine residues in solution I were comparatively less accessible to the quencher than those in solution II. Furthermore, in solution I, the protein was in a more compact conformation than the protein molecules in solution II.

These results, together with intrinsic fluorescence, indicated that protein molecules in solutions I and II were in different structural states. In the monomeric state, tyrosine residues are surface exposed; if two domains are associated with each other, these tyrosine residues should be buried. Hence, in both conditions, tyrosine residues possess different microenvironments, and ultimately different structural states. This also indicates the comparative compactness of protein in condition I. The difference in the acrylamide quenching may be due to the buried Tyr[19] in trimeric state, which is exposed in monomeric state (Fig. 4).

DLS

The hydrodynamic radius (R_H values) obtained in solution I (pH 7.4) was 3.0 ± 0.4 nm, whereas in solution II (pH 6.0) this was only 1.1 ± 0.1 nm (Fig. 3, *B* and *C*, Table 2). The lower value of polydispersity (4.3 ± 2.2% and 8.6 ± 3.1%, respectively) is a good sign of homogenous species in the solution. These values suggest that the N-terminal domain behaved as a trimer at physiological pH and monomer in acidic pH. The results from CD, fluorescence, and DLS experiments indicate clearly that at a physiological pH, the molecule exists in a trimeric state; at an acidic pH, it exists in its monomeric state. The addition of 20% ethanol at

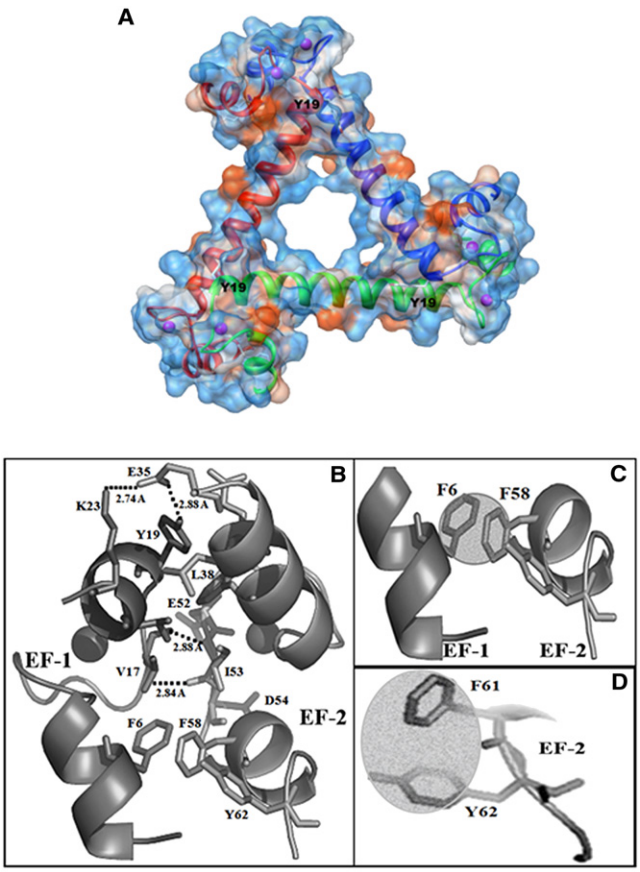

FIGURE 4 (*A*) Surface-view of domain-swapped trimer of Nt-EhCaBP1 showing Y19 in the hydrophobic-pocket involved in the formation of assembled-domain. The graphics were generated by Chimera (31). (*B*) Residues at interface of assembled domain Y19 in the hydrophobic-pocket of the assembled-domain can also be seen. (*C*) Interdomain and (*D*) intradomain π-π stacking in Nt-EhCBP1. The graphics were generated by PyMOL (30).

physiological conditions (solution I) resulted in the peak corresponding to the monomeric-form($R_H = 1 \pm 0.1$ nm) of the protein (Fig. 3 *D*), which is the result of the trimer-dissociation. The organic solvent ethanol must disturb the hydrophobic interactions between the trimeric interfaces.

Stability check of N-terminal domain

The fluorescence, CD, and DLS studies indicate that the two buffer conditions lead to two different structural states. In these two different structural states, they should also follow different denaturation or unfolding patterns. To verify this, denaturation studies were also carried out at these two conditions. Fig. 3 *inset* shows the fraction unfolded (f_D) protein curves of thermal unfolding transition for Nt-EhCaBP1 in different solution conditions measured by far-UV CD ($\theta_{222\ nm}$) and near-UV CD ($\theta_{280\ nm}$) to probe the unfolding of secondary and tertiary structures, respectively. We approximated the thermal denaturation transition in condition I as well as in condition II.

TABLE 3 Thermodynamic parameters for temperature induced transitions of Nt-EhCaBP1

Conditions	Variables	2° Structure (far-UV CD)	3° Structure (near-UV CD)
	m*	7.13 ± 0.12	7.39 ± 0.23
Trimer	T_m†	343.2 ± 2.5	334.9 ± 1.7
	$\Delta G_D(H_2O)$‡	2.5 ± 0.1	2.5 ± 0.1
	m	6.4 ± 0.1	6.5 ± 0.2
Monomer	T_m	337.3 ± 1.5	331.9 ± 1.8
	$\Delta G_D(H_2O)$	2.2 ± 0.1	2.2 ± 0.1

CD, circular dichroism; UV, ultraviolet.
*In cal $mol^{-1}K^{-1}$.
†In K.
‡In kcal mol^{-1}.

The denaturation curves show the pattern of T_m for secondary structural contents and tertiary contacts. The tertiary scaffold broke before the helical content disrupted in both conditions. The protein in condition I had a higher T_m than the monomeric protein in condition II (Table 3). It is clear from Fig. 3 *E* that ΔG_H linearly decreased as the temperature increased. This linear dependency is useful for quantitative comparison of temperature effect on these domains in different conditions. ΔG_D at starting temperature 20°C, $\Delta G_D(H_2O)$ was independent of secondary and tertiary structural probes; i.e., in case of trimer, the observed $\Delta G_D(H_2O)$ by both $\theta_{222\ nm}$ and $\theta_{280\ nm}$ was ~2.5 ± 0.1 kcal mol^{-1} and it was 2.2 ± 0.1 kcal mol^{-1} for monomer. Hence, the observed conformational stability of Nt-EhCaBP1 at 20°C was between 2.0 and 2.5 kcal mol^{-1}.

For trimer, the dependence of ΔG_D on temperature (m values) was greater than the values of monomer. The surface view of the trimeric organization of Nt-EhCaBP1 is shown in Fig. 4 *A*. In case of trimer (at pH 7.4), the major barriers to conformational transition were dissociation of N-terminal domains into its monomeric subunits at three positions associated with each other by interdomain hydrophobic/van der Waal/H-bonding/π-π interactions (Fig. 4, *B* and *C*). This dissociation was followed by disruption of individual N-terminal domain by weakening of intradomain interactions. The above finding explains why the denaturation of trimer is more cooperative than that of monomer. Furthermore, the value of m can also explain the solvent accessible surface residues (25). Hence, the difference in m is due to the interface residues buried in the trimer, but exposed in monomer.

Furthermore, it is clear from Fig. 5 *A* that the hydrophobic pocket formed at the interface of EF-1 and EF-2 of two N-terminal domains was stabilized by hydrophobic contacts, along with electrostatic interactions, van der Wall forces, and H-bonds in the trimeric state. The stability of these trimers was anticipated by π-π interaction between Phe^6 and Phe^{58} (Fig. 4 *D*). In monomeric states, these interactions do not exist; this may explain the variation in melting temperature.

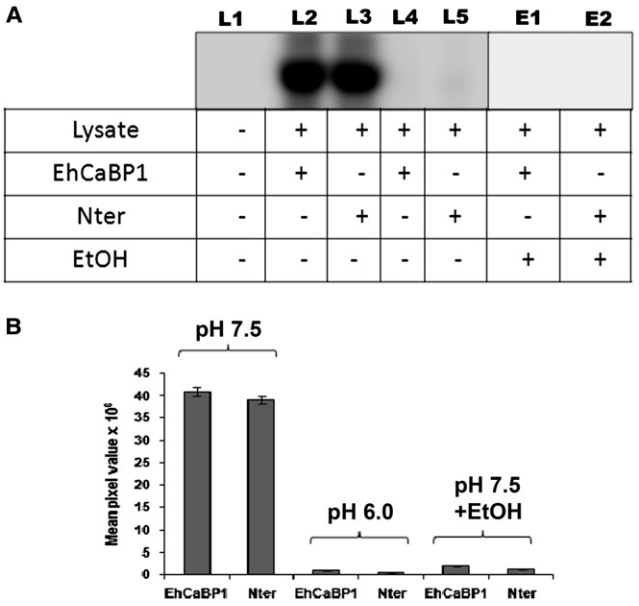

FIGURE 5 Endogenous kinase activation by full-length EhCaBP1 and its N-terminal domain. (*A*) *E. histolytica* cell-free lysate (25 ❍g) was the source of kinase and histone type III (15 mg) was the substrate. L2 and L3 represent EhCaBP1and Nter, respectively, at pH 7.5. L4 and L5 represent EhCaBP1and Nter, respectively, at pH 6.0. L6 and L7 represent EhCaBP1 and Nter, respectively, at pH 7.5 in presence of 20% ethanol. Two nanomoles of the protein concentration was used for the assay. The kinase assay was carried out using [γ_0-32P] ATP as the phosphate donor. The concentration of Ca^{2+} used was 10 ❍M. The reaction products were separated on a 14% SDS-PAGE and air dried; autoradiography was carried out. The first lane is histone alone. (*B*) The intensity of the autoradiogram was measured by densitometry, as represented by the bar diagram. The bar diagram shows the relative mean intensity ± standard deviation of three independent experiments.

Kinase activation

EhCaBP1 and Nt-EhCaBP1 activate endogenous kinase(s) in a Ca^{2+}-dependent manner (10,11). The ability of the full-length protein and its N-terminal domain to activate these kinase(s) was tested at pH 7.4 and pH 6.0, respectively, using histone phosphorylation visualized by autoradiography (10,26) (Fig. 5 *A*). Both Nt-EhCaBP1 and full-length EhCaBP1 could activate the endogenous kinase more efficiently at pH 7.4, as observed previously (10), but both proteins nearly lost their kinase activation function at pH 6.0 and in the presence of 20% ethanol at pH 7.4 (Fig. 5), indicating that the monomeric protein lost the power of target binding and activation.

CONCLUSIONS

The crystal structure of Nt-EhCaBP1 at 2.5 Å resolution represents a unique EF-hand assembly and domain-swapped trimerization. This crystal structure further validates the crystal structure of full-length EhCaBP1 reported previously from our laboratory. In that structure, only the N-terminal region was traced, and the C-terminal domain with central linker was missing (7). Even though the Nt-EhCaPB1 structure and full EhCaBP1 structures are very similar, the crystallization conditions of full-length and N-terminal domain are completely different indicating the involvement of C-terminal region in full-length EhCaBP1. Very few crystal structures of calcium-binding proteins with domain-swapped EF-hand organization have been reported, however, we believe trimerization has now been reported for the first time. Overall, the crystal structure of Nt-EhCaBP1 represents a unique example of how a molecule uses the structural motif of a similar molecule for domain formation and its functional variation.

As described before, couple of critical differences in the sequence between the two corresponding calcium-binding loops must be resulting in a remarkable change in the overall structural organization (7), but the basic functional motif retains its structural integrity for the molecule to function with a similar mode of target binding. The dynamic behavior of this domain was confirmed and the trimeric organization was validated at physiological conditions. Taking into consideration the solution structure of the full-length EhCaBP1 as monomeric at pH 6.0 (8), the dynamic behavior of Nt-EhCaBP1 was studied using circular dichroism spectroscopy, fluorescence spectroscopy, and dynamic light scattering experiments at pH 7.4 and pH 6.0. We believe these studies show clearly that Nt-EhCaBP1 exists as trimer at pH 7.4 and as monomer at pH 6.0.

Generally, many proteins exhibit variations in the kinetics, binding affinity and even multimeric nature with changes in pH from 6.0 to 7.5. In almost all the cases a histidine residue is involved in these processes, which has pK_a in this range. Interestingly, Nt-CaBP1 does not have single histidine residue but still changes its multimeric nature and structure. Individually, each amino acid plays a significant role in imparting a proper conformation to a protein because of its intrinsic helix-forming, helix-breaking, sheet-forming, and sheet breaking propensity (27). The mere secondary structure forming intrinsic propensity of an individual amino acid, however, is not enough to determine the structural fate of a nascent polypeptide chain. The microenvironment of a residue is the main deciding parameter for protein conformation. Ionic residues are highly negatively/positively charged at neutral pH; by electrostatic attraction/repulsion, they tend to orient the polypeptide backbone so that the H-bonding pattern can be rearranged to obtain altered secondary structural elements. Nt-EhCaBP1 is a protein rich in charged amino acids (33%) with respect to its low content of hydrophobic residues. In other words, this protein is conformationally flexible in aqueous solution with respect to its quaternary structures. The transition from a trimeric to a monomeric state is associated with a large positive heat capacity change, which correlates with the ordering of water around nonpolar groups that become exposed to solvent after being on the interior of the protein in the native state. Hence, the entropy gained by not ordering the water around

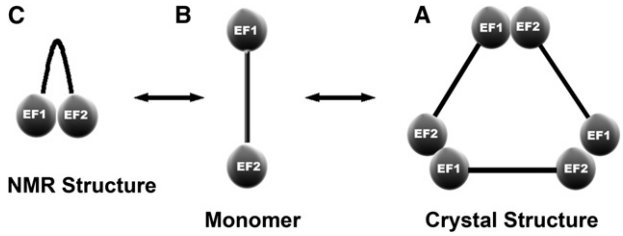

FIGURE 6 Model of the dynamic equilibrium of Nt-EhCaBP1. (*A*) At physiological conditions (pH 7.4), the protein molecule exists as a trimer as seen in crystal structure. (*B*) Low pH (pH 6.0) leads to the dissociation of trimer to its monomeric units. (*C*) NMR structure of the N-terminal region of full-length EhCaBP1 is also shown where EF-1 and EF-2 are closely associated and forming the N-terminal domain of the full-length protein.

nonpolar side chains of interfacing residues certainly counteracts a great deal of the entropy gained by their exposure to the solvent. This protein can be induced to fold in more compact structures with an increase in ordered secondary structural contents, especially α-helical segments in physiological conditions; hydrophobic interactions are extremely high in Nt-EhCaBP1, and the elevated level of H^+ enhances local rearrangement of forces associated with every type of interaction. Hence, the preferred orientation and conformation of protein is adopted according to the requirement for binding of metal ions, small peptides, and drugs to this protein. Usually, different conditions of temperature solvent and pH of the medium lead to trimer-monomer transition. The alteration in pH results in a charge neutralization of extremely higher proportion of charged residues. It would have facilitated the formation of a monomeric from trimeric status (Fig. 6) with lower helix content and higher random coil structure, as well as partial hydrophobic collapse, in accordance with Holtzer and Holtzer (28), who treated the helix-coil transition coupled with a dimer-monomer transition. These studies help to explain how these models physically perform when the side chains go from rigid to nonrigid packing. The above unusual characteristics of Nt-EhCBP1 motivated us to carry out further structural studies to obtain a clear picture of unique orientation and phase transition of related calcium binding proteins.

On the basis of the available structural information, Nt-EhCaBP1 can be represented in three models, as shown in Fig. 6. At the physiological condition, Nt-EhCaBP1 exists as a trimer, as observed in the crystal structure (Fig. 6 *C*); at a low pH, the trimer dissociates into its monomeric unit (Fig. 6, *A* and *B*). The model represents the two monomeric forms, one with a long extended helix separating the two EF-hand motifs (Fig. 6 *B*), and the other with the EF-hand motifs closely associated and with extensive hydrophobic contacts, as reported in the NMR structure of this protein (Fig. 6 *A*). The spectroscopic observations at low pH indicate a state with exposed hydrophobic surface, which is possible if the protein adopts the conformation shown in Fig. 6 *B*; the CD experiments confirm a lower α-helical content at lower pH, which can be similar to NMR structure, where the helix between the EF-hand motifs is distorted, but the exposed hydrophobic surface is not supported in NMR structure. We believe these results indicate clearly the existence of an intermediate or equilibrium state between the long extended helix monomer structure and the NMR structure at low pH.

In the monomeric form of Nt-EhCaBP1 at pH. 6.0, or in the presence of 20% ethanol, the protein loses the endogenous kinase activation function. In the monomeric form of the protein, the EF hand motifs are separated. It is well known that the single EF hand motifs are not functional; only when they are paired can they become functional and bind to the targets (29). Thus, H^+ induced conformational changes from trimer $\rightarrow$ monomer may be used to unveil the mechanism of action and mode of function in cell signaling. The *E. histolytica* might have this kind of regulation, where even if the required calcium levels are present to activate EhCaBP1, if the environment is acidic, it will not activate the kinases; thus, it may inhibit phagocytosis.

SUPPORTING MATERIAL

Two figures are available at http://www.biophysj.org/biophysj/supplemental/S0006-3495(10)00414-5.

We express our deep appreciation to Prof. A. Bhattacharya, School of Life Sciences, Jawaharlal Nehru University, New Delhi, for his support. Advanced Instrumentation Research Facility, Jawaharlal Nehru University, is acknowledged for access to XRD and CD instruments.

This study was supported by Department of Science and Technology, Government of India, and Innovative Young Biotechnology Award of Department of Biotechnology. S.K. thanks University Grants Commission. S.K. and M.S.M. thank Council of Scientific Industrial Research, Government of India, for fellowship.

REFERENCES

1. WHO/PAHO/UNESCO. 1997. WHO/PAHO/UNESCO report. A consultation with experts on amoebiasis. Mexico City, Mexico 28-29 January, 1997. *Epidemiol. Bull.* 18:13–14.
2. WHO/PAHO/UNESCO report (WHO, Mexico). 1997. A consultation with experts on Amoebiasis. *Epidemiol. Bull.* 18:13–14.
3. Stanley, Jr., S. L. 2003. Amoebiasis. *Lancet.* 361:1025–1034.
4. Loftus, B., I. Anderson, …, N. Hall. 2005. The genome of the protist parasite *Entamoeba histolytica*. *Nature.* 433:865–868.
5. Bhattacharya, A., N. Padhan, …, S. Bhattacharya. 2006. Calcium-binding proteins of *Entamoeba histolytica*. *Arch. Med. Res.* 37: 221–225.
6. Sahoo, N., E. Labruyère, …, A. Bhattacharya. 2004. Calcium binding protein 1 of the protozoan parasite *Entamoeba histolytica* interacts with actin and is involved in cytoskeleton dynamics. *J. Cell Sci.* 117:3625–3634.
7. Kumar, S., N. Padhan, …, S. Gourinath. 2007. Crystal structure of calcium binding protein-1 from *Entamoeba histolytica*: a novel arrangement of EF hand motifs. *Proteins.* 68:990–998.
8. Atreya, H. S., S. C. Sahu, …, G. Govil. 2001. NMR derived solution structure of an EF-hand calcium-binding protein from *Entamoeba Histolytica*. *Biochemistry.* 40:14392–14403.

9. Babu, Y. S., J. S. Sack, …, W. J. Cook. 1985. Three-dimensional structure of calmodulin. *Nature*. 315:37–40.
10. Jain, R., S. Kumar, …, A. Bhattacharya. 2009. N- and C-terminal domains of the calcium binding protein EhCaBP1 of the parasite *Entamoeba histolytica* display distinct functions. *PLoS One*. 4:e5269.
11. Yadava, N., M. R. Chandok, …, A. Bhattacharya. 1997. Characterization of EhCaBP, a calcium-binding protein of *Entamoeba histolytica* and its binding proteins. *Mol. Biochem. Parasitol*. 84:69–82.
12. Prasad, J., S. Bhattacharya, and A. Bhattacharya. 1993. The calcium binding protein of *Entamoeba histolytica*: expression in *Escherichia coli* and immunochemical characterization. *Cell. Mol. Biol. Res.* 39:167–175.
13. Bradford, M. M. 1976. A rapid and sensitive method for the quantitation of microgram quantities of protein utilizing the principle of protein-dye binding. *Anal. Biochem.* 72:248–254.
14. Storoni, L. C., A. J. McCoy, and R. J. Read. 2004. Likelihood-enhanced fast rotation functions. *Acta Crystallogr. D Biol. Crystallogr*. 60:432–438.
15. Emsley, P., and K. Cowtan. 2004. Coot: model-building tools for molecular graphics. *Acta Crystallogr. D Biol. Crystallogr*. 60: 2126–2132.
16. Brünger, A. T., P. D. Adams, …, G. L. Warren. 1998. Crystallography and NMR system: a new software suite for macromolecular structure determination. *Acta Crystallogr. D Biol. Crystallogr*. 54:905–921.
17. Adams, P. D., R. W. Grosse-Kunstleve, …, T. C. Terwilliger. 2002. *PHENIX*: building new software for automated crystallographic structure determination. *Acta Crystallogr. D Biol. Crystallogr*. 58: 1948–1954.
18. Johnson, Jr., W. C. 1990. Protein secondary structure and circular dichroism: a practical guide. *Proteins*. 7:205–214.
19. Haq, S. K., S. Rasheedi, and R. H. Khan. 2002. Characterization of a partially folded intermediate of stem bromelain at low pH. *Eur. J. Biochem*. 269:47–52.
20. Chakrabarty, P., D. K. Sethi, …, A. Bhattacharya. 2004. Identification and characterization of EhCaBP2. A second member of the calcium-binding protein family of the protozoan parasite *Entamoeba histolytica*. *J. Biol. Chem*. 279:12898–12908.
21. Kleywegt, G. J., and A. T. Brünger. 1996. Checking your imagination: applications of the free R value. *Structure*. 4:897–904.
22. Andrade, M. A., P. Chacón, …, F. Morán. 1993. Evaluation of secondary structure of proteins from UV circular dichroism spectra using an unsupervised learning neural network. *Protein Eng*. 6: 383–390.
23. Merelo, J. J., M. A. Andrade, …, F. Morán. 1994. Proteinotopic feature maps. *Neurocomputing*. 6:443–454.
24. Stryer, L. 1965. The interaction of a naphthalene dye with apomyoglobin and apohemoglobin. A fluorescent probe of non-polar binding sites. *J. Mol. Biol*. 13:482–495.
25. Myers, J. K., C. N. Pace, and J. M. Scholtz. 1995. Denaturant m values and heat capacity changes: relation to changes in accessible surface areas of protein unfolding. *Protein Sci*. 4:2138–2148.
26. Jain, R., J. Santi-Rocca, …, A. Bhattacharya. 2008. Calcium-binding protein 1 of *Entamoeba histolytica* transiently associates with phagocytic cups in a calcium-independent manner. *Cell. Microbiol*. 10:1373–1389.
27. Chou, P. Y., and G. D. Fasman. 1978. Prediction of the secondary structure of proteins from their amino acid sequence. *Adv. Enzymol. Relat. Areas Mol. Biol*. 47:45–148.
28. Holtzer, M. E., and A. Holtzer. 1990. α-helix to random coil transitions of two-chain coiled coils: experiments on the thermal denaturation of isolated segments of α α-tropomyosin. *Biopolymers*. 30:985–993.
29. Grabarek, Z. 2006. Structural basis for diversity of the EF-hand calcium-binding proteins. *J. Mol. Biol*. 359:509–525.
30. DeLano, W. L. 2002. The PyMOL User's Manual. DeLano Scientific, San Carlos, CA.
31. Pettersen, E. F., T. D. Goddard, …, T. E. Ferrin. 2004. UCSF Chimera—a visualization system for exploratory research and analysis. *J. Comput. Chem*. 25:1605–1612.